

Magnon-induced high-order sideband generation

Zeng-Xing Liu, Bao Wang, Hao Xiong,* and Ying Wu

School of physics, Huazhong University of Science and Technology, Wuhan 430074, China

(Dated: May 3, 2019)

Magnon Kerr nonlinearity plays crucial roles in the study of cavity optomagnonics system and may bring many novel physical phenomena and important applications. In this work, we report the investigation of high-order sideband generation induced by magnon Kerr nonlinearity in a cavity-magnon system, which is critically lacking in this emerging research field. We uncover that the driving field plays a significant role in controlling the generation and amplification of the higher-order sidebands and the sideband spacing can be adjusted by regulating the beat frequency between the pump laser and the probe laser, which is extremely eventful for the spacing modulation of the sideband spectrum. Based on the recent experimental progress, our results deepen our cognition into optomagnonics nonlinearity and may find interesting applications in optical frequency metrology and optical communications.

PACS numbers: 42.50.Pq, 42.65.Ky

Cavity-magnon system has recently been the subject of extensive investigations and made great achievements in the past few years [1–10]. Figure 1(a) shows a schematic diagram of a typical cavity-magnon system, in which a millimeter-scale magnetic insulator yttrium iron garnet (YIG) [11] is loaded in a high-finesse microwave cavity. Under the bias magnetic field, the YIG crystal gives rise to a new polaritons state [12–14] called magnons. The coherent coupling between the magnons and microwave photons [15–19], superconducting qubits [20, 21], electron [22] and phonons [23] has been experimentally demonstrated, which can selectively utilize the special advantages from different physical systems to better explore newest physical phenomena. Recently, a up-and-coming conception magnon-based computing circuits [24] has been proposed and the magnons have potential for the implementation of alternative computing concepts [25]. In addition, cavity-magnon system has opened up avenues of providing a new platform to establish quantum information network thanks to the long coherence time of both magnons and microwave photons [1–3]. An important example is that the magnon dark modes can be utilized to build a magnon gradient memory [26] to store information at room temperature, which opened the curtain in the application of quantum information processing based on cavity-optomagnonic system.

To our knowledge, however, the current research often ignore optomagnonics nonlinear effect [1–3, 8–10] which will lead to some interesting phenomena such as magnon soliton [27] and magnon sidebands [28], so further insight into the nonlinear regime may open up a new and broad prospective for the properties of the cavity-magnon system. Recently, the concept of magnon Kerr nonlinearity, originating from the magnetocrystalline anisotropy in the YIG [29, 30], has been introduced in a strongly coupled cavity-magnon system, and the nonlinearity-induced frequency shift has been experimentally demonstrated [31]. Furthermore, the bistability of cavity magnon polaritons has also been experimentally confirmed

[32]. These pioneering works establish the experimental foundation to explore nonlinear characteristics in this emerging field. In this work, we investigate high-order sideband generation induced by magnon Kerr nonlinearity in a cavity-magnon system, which is critically lacking in this emerging research area. The high-order sideband is a comb-like spectral structure containing a series of equidistant frequency components. As shown in Fig. 1(b), a pump laser with frequency ω_1 and a probe laser with frequency ω_p are incident on the cavity field, and then the output field will generate a series of sidebands with equidistant frequency $\mathcal{F}_n = \omega_1 \pm n\Delta$ where Δ is the beat frequency of the pump laser and the probe laser, and n is an integer that represents the order of the sidebands. Compared with high-order sideband generation (HSG) in optomechanical system [33, 34], we found that the magnon-induced high-order sideband generation (MHSG) proposed here has some special features. For example, the generation and amplification of MHSG does not satisfy the linear relationship with the power of the control field because the magnon Kerr nonlinearity will reach saturation when the driving power exceeds a certain threshold. An optimal power area, about 12 mW, is proposed which may have potential applications in low-power optical frequency combs. More interestingly, the sideband spacing of MHSG maybe arbitrarily adjusted by harnessing the beat frequency which is of great significance for improving the measurement accuracy of the frequency-combs-based sensor. So our scheme may not only deepen our understanding of optomagnonics nonlinear interactions but also find applications in optical frequency metrology [35–37].

The physical setup under investigation is a hybrid magnon-cavity system, as schematically shown in Fig. 1(a). The YIG crystal is directly driven by a microwave source at frequency ω_d and the driving strength $\xi_d = \sqrt{\gamma_m P_d / (\hbar \omega_d)}$ with P_d the power of the control field and γ_m the decay rate of the magnon mode. The cavity field is probed by a weak bichromatic input field, a pump field (central frequency ω_1 , pump power P_1 , and amplitude $\xi_1 = \sqrt{\kappa P_1 / (\hbar \omega_1)}$ with the decay rate κ) and a probe field (central frequency ω_p , probe power P_p , and amplitude $\xi_p = \sqrt{\kappa P_p / (\hbar \omega_p)}$). Under the rotating wave approximation, the Hamiltonian of the whole system in a frame rotating at

*Electronic address: haoxiong1217@gmail.com

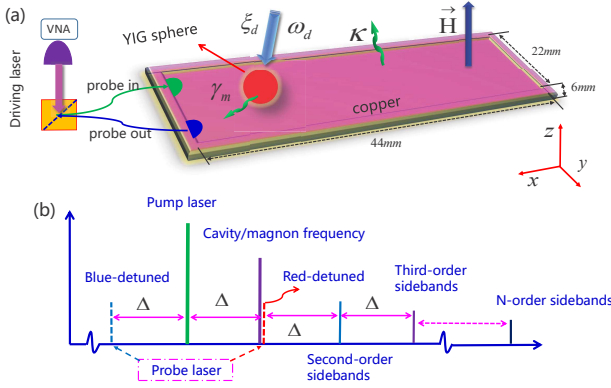


FIG. 1: (Color online) (a) Schematic diagram of a cavity-magnon system. A small YIG sphere, driven by a strong microwave source with the drive strength ξ_d and frequency ω_d , is glued to a three-dimensional copper microwave cavity with dimensions $44 \times 22 \times 6$ mm³ [32]. A weak bichromatic probe laser consisting of a pump field and a probe field is input the cavity via the green port and output via the blue port. The transmission spectra can be recorded by a vector network analyzer (VNA). A bias magnetic field with magnetic strength H is applied along the z direction. (b) Frequency spectrogram output from the cavity-magnon system. The frequency of the pump laser is shown by the green line, while the cavity (magnon) frequency is shown purple line. The blue dashed (blue-detuning) and red dotted lines (red-detuning) indicate the probe laser (here we only discuss the latter case), and Δ is the beat frequency between the pump laser and the probe laser. There are second-, third-, and n -order sidebands generation.

frequency ω_l of the pump field can be written as [31]

$$\begin{aligned} \hat{H} = & \hbar\Delta_a\hat{a}^\dagger\hat{a} + \hbar\Delta_b\hat{b}^\dagger\hat{b} + \hbar\mathcal{K}\hat{b}^\dagger\hat{b}\hat{b}^\dagger\hat{b} \\ & + \hbar\mathcal{G}(\hat{a}\hat{b}^\dagger + \hat{a}^\dagger\hat{b}) + i\hbar\xi_d(\hat{b}^\dagger e^{-i\Delta_b t} - \hat{b}e^{i\Delta_b t}) \\ & + i\hbar\xi_l(\hat{a}^\dagger - \hat{a}) + i\hbar\xi_p(\hat{a}^\dagger e^{-i\Delta t} - \hat{a}e^{i\Delta t}), \end{aligned} \quad (1)$$

where $\Delta_{a(b)} = \omega_{a(b)} - \omega_l$ being the frequency detuning of the cavity (magnon) mode relative to the pump field and $\Delta = \omega_p - \omega_l$ being the beat frequency between the pump laser and the probe laser. \hat{a} (\hat{a}^\dagger) and \hat{b} (\hat{b}^\dagger), respectively, are the annihilation (creation) operators of the microwave cavity mode at frequency ω_a and the magnon mode at frequency ω_b . The term $\hbar\mathcal{K}\hat{b}^\dagger\hat{b}\hat{b}^\dagger\hat{b}$ represents the magnon Kerr effect, where $\mathcal{K} = \mu_0\mathcal{K}_0\varrho^2/(\mathcal{M}^2\mathcal{V}_m)$ with μ_0 the magnetic permeability of free space, \mathcal{K}_0 the first-order anisotropy constant, ϱ the gyromagnetic ratio, \mathcal{M} the saturation magnetization, and \mathcal{V}_m the volume of the YIG sphere [31]. \mathcal{G} is the magnon-photon coupling strength and, here, $\mathcal{G} > \kappa, \gamma_m$, i.e., the system falls in the strong-coupling regime. Note that the Kerr coefficient \mathcal{K} is inversely proportional to \mathcal{V}_m so the magnon Kerr nonlinearity can be strengthened when reducing \mathcal{V}_m . In this work, we are interested in the mean response of the system, so the operators can be reduced to their expectation values, viz., $\alpha(t) \equiv \langle \hat{a}(t) \rangle$ and $\beta(t) \equiv \langle \hat{b}(t) \rangle$. With cavity field and magnon mode damping processes included, the evolution of the hybrid cavity-magnon system can be described by the Heisenberg-Langevin

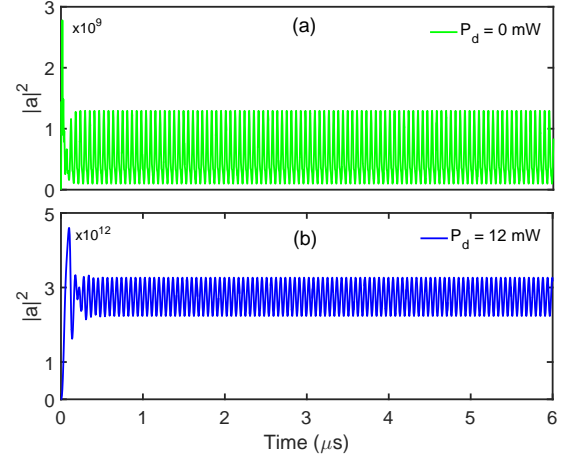


FIG. 2: (Color online) Time evolution of microwave photon number $|\alpha|^2$ of the cavity field (a) in the absence of driving YIG crystal and (b) in the presence of driving YIG crystal. The parameters used in numerical simulation are $\omega_a/2\pi = \omega_b/2\pi = 10.1$ GHz, $\kappa/2\pi = 3.8$ MHz, $\gamma_m/2\pi = 17.5$ MHz, $\mathcal{G}/2\pi = 41$ MHz, $\mathcal{K}/\kappa = 10^{-10}$, $\Delta_a = \Delta_b = \Delta = \gamma_m$, $P_l = P_p = 6.9$ μ W. All the parameters are chosen based on the latest experiment [32].

equations as

$$\begin{aligned} \dot{\alpha} &= (-i\Delta_a - \frac{\kappa}{2})\alpha - i\mathcal{G}\beta + \xi_l + \xi_p e^{-i\Delta t}, \\ \dot{\beta} &= (-i\Delta_b - \frac{\gamma_m}{2})\beta - i(2\mathcal{K}\beta^*\beta + \mathcal{K})\beta - i\mathcal{G}\alpha + \xi_d e^{-i\Delta_b t}. \end{aligned} \quad (2)$$

Here, the mean-field approximation by factorizing averages is used, i.e., $\langle \alpha\beta \rangle \equiv \langle \alpha \rangle \langle \beta \rangle$, and the quantum noise terms can be dropped safely because their expectation values are zero in the semiclassical approximation.

The microwave photon number $|\alpha|^2$ of the cavity field can be obtained by solving Eqs. (2), and we plot the time evolution of $|\alpha|^2$ in Fig. 2. We can see that when the system reaches a stable oscillation after a transient process, the number of microwave photons in the cavity is relatively small in the absence of driving the YIG crystal (Fig. 2 (a)), however, when the YIG crystal is driven, the photon number of the cavity is greatly increased (Fig. 2 (b)). A considerable magnons will generate when the YIG crystal is pumped and the magnon Kerr effect yields a strong nonlinearity to the system [31] which will enhance the interaction between magnons and photons. Next, we discuss high-order sideband generation from the cavity-magnon system. The output field $s_{out}(t)$ can be obtained by using the input-output relation, and the output spectrum $\mathcal{S}(\omega)$ in frequency domain can be acquired by performing the fast Fourier transform of $s_{out}(t)$, i.e.,

$$\mathcal{S}(\omega) = \left| \frac{1}{2\pi} \int_{-\infty}^{\infty} s_{out}(t) e^{-i\omega t} dt \right| \quad (3)$$

where ω is the spectroscopy frequency from the output field. After doing the fast Fourier transform, the frequency spectrum of the output field will appear the second-, third- and higher-order sidebands.

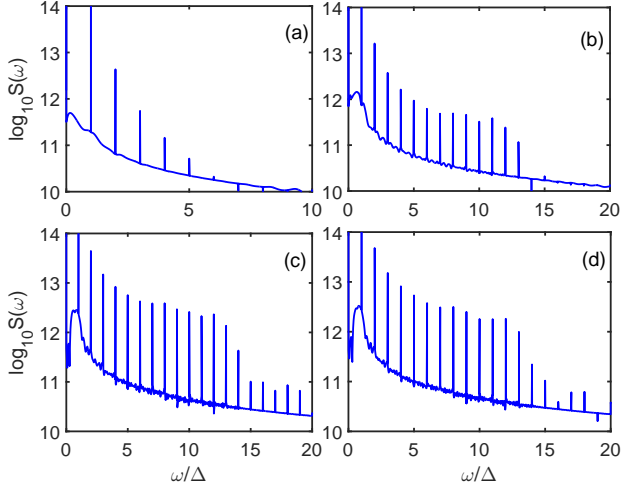


FIG. 3: (Color online) The MHS spectra output from the cavity-magnon system is shown with different powers of the control field P_d . (a) $P_d = 1$ mW, (b) $P_d = 5$ mW, (c) $P_d = 12$ mW, (d) $P_d = 15$ mW. The other parameters for simulation are the same as those in Fig. 2.

Figure 3 shows how the control field can be used to overmaster the generation and amplification of MHS. As shown in Fig. 3(a), the weak control laser ($P_d = 1$ mW) only induced a few low-order sidebands. Under this condition, the magnon Kerr-nonlinearity process is very weak and the generated high-order sideband are almost absorbed. In Fig. 3(b), we increase the control field power to $P_d = 5$ mW, both the order and intensity of the sidebands have been strengthened which means that the magnon Kerr nonlinearity reinforces with the increase of control power. To further investigate the effects of the control field on MHS, we increase the power of the control laser $P_d = 12$ mW which shows that a series of robust sidebands appear in the frequency spectrum. The spectrum structure of MHS is that it decreases rapidly for the first few order sidebands and follows by a plateau where all the sidebands have the same strength, and until by a cut-off regime where the amplitude of the sidebands decreases sharply to complete this spectrum. In addition, some non-perturbative signs emerge on the sideband spectrum that is the intensity of the lower-order sidebands have smaller than the higher-order sidebands, which indicates that a strong nonlinearity be produced from the YIG crystal under the drive field. Continuing to increase the power of control field $P_d = 15$ mW, the MHS spectrum as shown in Figs. 3(d), however, both the cutoff order and the amplitude of the higher-order sidebands do not strengthen as the power increases which means that the magnon Kerr-nonlinearity intensity is no longer increased but suppressed when the driving power exceeds a certain threshold. This result reminds us of the possibility of bridling the magnon nonlinear strength by adjusting the power of the control field, and further achieve the purpose of harnessing the sideband spectrum, which may have potential applications in low-power optical frequency combs [38, 39] and optical communications, as [40] has suggested.

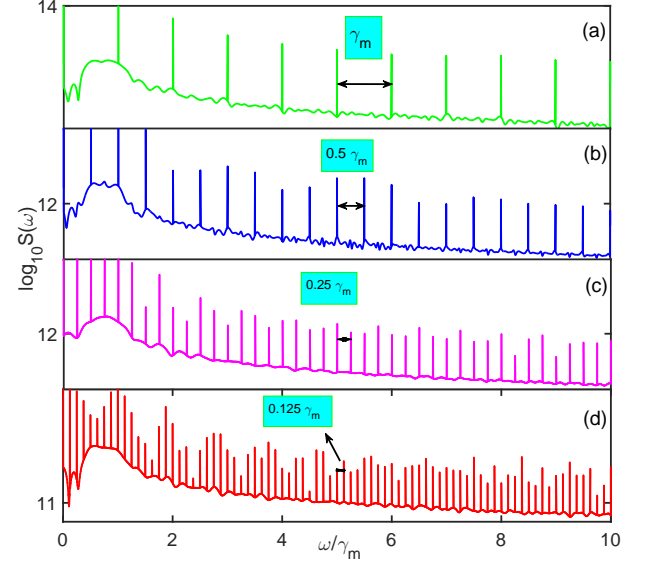


FIG. 4: (Color online) The MHS spectra output from the cavity-magnon system is shown with different beat frequency Δ . (a) $\Delta/\gamma_m = 1$, (b) $\Delta/\gamma_m = 0.5$, (c) $\Delta/\gamma_m = 0.25$, (d) $\Delta/\gamma_m = 0.125$. The other parameters for simulation are the same as those in Fig. 2(b).

Realizing sideband-spacing adjustment is of fundamental importance in optical frequency metrology [35–37]. We uncovered that the sideband spacing in our scheme can be adjusted by regulating the beat frequency between the pump laser and the probe laser while the sideband spacing of HSG in optomechanical system is unchangeable due to the inherent frequency of the oscillator, as [33, 34] manifestation. In Fig. 4, we plot the MHS spectra with four different values of the beat frequency Δ . It is clearly shown that as the beat frequency decreases, the spacing of the MHS spectra becomes narrower and narrower. For convenience, we only discuss the case that the sideband order before $\omega/\gamma_m = 10$. For the case of $\Delta/\gamma_m = 1$ in Fig. 4(a), the number of sidebands is 10 and the spacing of each sideband is γ_m . For the case of $\Delta/\gamma_m = 0.5$ in Fig. 4(b), however, the number of sidebands is increased to 20 while the spacing of each sideband is decreased to $0.5\gamma_m$, which is half as wide as in Fig. 4(a). Further decrease the beat frequency $\Delta_p/\gamma_m = 0.25$ in Fig. 4(c), the amount of sidebands is increasing fourfold and the spacing of each sideband is as narrow as $0.25\gamma_m$. A more cramped sideband spacing can be obtained as we continue to decrease the beat frequency $\Delta_p/\gamma_m = 0.125$, as Fig. 4(d) shown. From above discussion, we can see that the beat frequency indeed plays an important role in the modulation of the sidebands spacing, which reminds us of the possibility of implementing the sideband spectrum with arbitrary spacing, so our scheme may has important applications in spectral precision measurement, as [35–37] recommendation.

Here, it is worth emphasizing that such magnon-induced high-order sideband generation in our scheme has several distinctive advantages. First, our system is a brand new magneto-optical system, which has some unusual merits. For instance, the system has rich magnonic nonlinearities and very low loss

for various different information carriers even at room temperature [41], which may provide environmental conditions for real applications of MHSg. Moreover, the cavity magnonics system possesses the advantages of tunability and compatibility with opto- or electromechanical elements, providing an excellent platform for quantum state transfer among different physical systems, as [23] has shown. Second, we find that the generation and amplification of MHSg can be modulated by the control field and an optimal power region has been proposed, which may find application in low-power frequency combs. In particular, the MHSg spacing is directly determined by the frequency difference Δ between the pump laser and the probe laser, namely, the sideband spectra may be regulated in arbitrary spacing. So our scheme may trigger substantial advances in practical application of high-order sidebands in optical frequency metrology and optical communications, as [40] proposal. Finally, to our knowledge, the investigation of high-order sideband generation induced by magnon Kerr nonlinearity is still in blank in previous research, so this work may enable deepen our understanding in optomagnonics nonlinearity and may open up a broad prospective for the nonlinear properties of the cavity-magnon system.

Ultimately, it is necessary to evaluate the actual experimental possibilities of the MHSg. The present scheme could be realized under the state-of-the-art experimental conditions. First of all, we note that the Kerr coefficient \mathcal{K} is inversely proportional to \mathcal{V}_m , thence the Kerr effect will bring strong nonlinearity when using a small YIG sphere in the cavity-magnon system. Under the current experimental technology, the YIG crystal can be made into a highly polished sphere with diameter as small as $250\ \mu\text{m}$ [23], and such small YIG sphere can

bring a sufficiently strong Kerr nonlinearity when we driving the YIG sample. Furthermore, the magnons can be tuned by an external magnetic field and the magnon-photon coupling can be tuned by moving the YIG sphere inside the cavity. In Ref. [31], the external magnetic field is tunable in the range of 0 to 1 T and the frequency of the magnon mode is adjustable ranges from several hundreds of megahertz to 28 GHz, such wide frequency range allows the resonance coupling between the magnons and microwave photons (in Ref. [3], a high cooperativity $C = 4\mathcal{G}^2/\kappa\gamma_m = 3.0 \times 10^3$ has been achieved). Therefore, our program proposed here can easily be implemented under the current experimental conditions.

In summary, an important nonlinear phenomenon: high-order sideband generation, induced by magnon Kerr nonlinearity in a strongly coupled cavity-magnon system has been uncovered, which is critically lacking in this emerging research field. We shown that the generation and amplification of the higher-order sidebands can be modulated by bridling the control field and an optimal power area, about 12 mW, is proposed. In addition, we found that the the beat frequency between the pump laser and the probe laser plays critical role in sideband-spacing adjustment. Beyond their fundamental scientific significance, our results may have potential applications in optical frequency metrology and optical communications.

The work was supported by National Key Research and Development Program of China (2016YFA0301203), and the National Natural Science Foundation of China (NSFC) (11774113, 11374116, 11574104, 11375067).

-
- [1] H. Huebl, C. W. Zollitsch, J. Lotze, F. Hocke, M. Greifenstein, A. Marx, R. Gross, and S. T. B. Goennenwein, *Phys. Rev. Lett.* **111**, 127003 (2013).
 - [2] M. Goryachev, W. G. Farr, D. L. Creedon, Y. Fan, M. Kostylev, and M. E. Tobar, *Phys. Rev. Applied* **2**, 054002 (2014).
 - [3] Y. Tabuchi, S. Ishino, T. Ishikawa, R. Yamazaki, K. Usami, and Y. Nakamura, *Phys. Rev. Lett.* **113**, 083603 (2014).
 - [4] X. Zhang, C. L. Zou, L. Jiang, and H. X. Tang, *Phys. Rev. Lett.* **113**, 156401 (2014).
 - [5] Z. X. Liu, B. Wang, C. Kong, H. Xiong, and Y. Wu, *Appl. Phys. Lett.* **112**, 111109 (2018).
 - [6] L. Bai, M. Harder, Y. P. Chen, X. Fan, J. Q. Xiao, and C. M. Hu, *Phys. Rev. Lett.* **114**, 227201 (2015).
 - [7] B. Z. Rameshti, Y. Cao, and G. E. W. Bauer, *Phys. Rev. B* **91**, 214430 (2015).
 - [8] Ö. O. Soykal and M. E. Flatté, *Phys. Rev. Lett.* **104**, 077202 (2010).
 - [9] T. Liu, X. Zhang, H. X. Tang, and M. E. Flatté, *Phys. Rev. B* **94**, 060405 (2016).
 - [10] D. Zhang, X. M. Wang, T. F. Li, X. Q. Luo, W. Wu, F. Nori, and J. Q. You, *npj Quantum Inf.* **1**, 15014 (2015).
 - [11] A. A. Serga, A. V. Chumak, and B. Hillebrands, *J. Phys. D: Appl. Phys.* **43**, 264002 (2010).
 - [12] Y. Cao, P. Yan, H. Huebl, S. T. B. Goennenwein, and G. E. W. Bauer, *Phys. Rev. B* **91**, 094423 (2015).
 - [13] B. M. Yao, Y. S. Gui, Y. Xiao, H. Guo, X. S. Chen, W. Lu, C. L. Chien, and C. M. Hu, *Phys. Rev. B* **92**, 184407 (2015).
 - [14] V. V. Kruglyak, S. O. Demokritov, and D. Grundler, *J. Phys. D: Appl. Phys.* **43**, 264001 (2010).
 - [15] J. Bourhill, N. Kostylev, M. Goryachev, D. L. Creedon, and M. E. Tobar, *Phys. Rev. B* **93**, 144420 (2016).
 - [16] A. Osada, R. Hisatomi, A. Noguchi, Y. Tabuchi, R. Yamazaki, K. Usami, M. Sadgrove, R. Yalla, M. Nomura, and Y. Nakamura, *Phys. Rev. Lett.* **116**, 223601 (2016).
 - [17] X. Zhang, N. Zhu, C. L. Zou, and H. X. Tang, *Phys. Rev. Lett.* **117**, 123605 (2016).
 - [18] J. A. Haigh, A. Nunnenkamp, A. J. Ramsay, and A. J. Ferguson, *Phys. Rev. Lett.* **117**, 133602 (2016).
 - [19] C. Braggio, G. Carugno, M. Guarise, A. Ortolan, and G. Ruoso, *Phys. Rev. Lett.* **118**, 107205 (2017).
 - [20] Y. Tabuchi, S. Ishino, A. Noguchi, T. Ishikawa, R. Yamazaki, K. Usami, and Y. Nakamura, *Science* **349**, 405 (2015).
 - [21] D. Lachance-Quirion, Y. Tabuchi, S. Ishino, A. Noguchi, T. Ishikawa, R. Yamazaki, and Y. Nakamura, *Sci. Adv.* **3**, e1603150 (2017).
 - [22] E. Carpena, E. Mancini, C. Dallera, M. Brenna, E. Puppin, and S. D. Silvestri, *Phys. Rev. B* **78**, 174422 (2008).
 - [23] X. Zhang, C. L. Zou, L. Jiang, and H. X. Tang, *Sci. Adv.* **2**, e1501286 (2016).
 - [24] A. V. Chumak, V. I. Vasyuchka, A. A. Serga, and B. Hillebrands, *Nat. Phys.* **11**, 453 (2015).
 - [25] K. Wright, *Physics*, **11**, 23 (2018).

- [26] X. Zhang, C. L. Zou, N. Zhu, F. Marquardt, L. Jiang, and H. X. Tang, Nat. Commun. **6**, 8914 (2015).
- [27] J. Corones, Phys. Rev. B **16**, 1763.(1977).
- [28] M. O. Ramirez, A. Kumar, S. A. Denev, N. J. Podraza, X. S. Xu, R. C. Rai, Y. H. Chu, J. Seidel, L. W. Martin, S. Y. Yang, et al., Phys. Rev. B **79**, 224106 (2009).
- [29] D. D. Stancil and A. Prabhakar, *Spin Waves* (Springer, Berlin, 2009).
- [30] A. G. Gurevich and G. A. Melkov, *Magnetization Oscillations and Waves* (CRC, Boca Raton, FL, 1996).
- [31] Y. P. Wang, G. Q. Zhang, D. Zhang, X. Q. Luo, W. Xiong, S. P. Wang, T. F. Li, C. M. Hu, and J. Q. You, Phys. Rev. B **94**, 224410 (2016).
- [32] Y. P. Wang, G. Q. Zhang, D. Zhang, T. F. Li, C. M. Hu, and J. Q. You, Phys. Rev. Lett. **120**, 057202 (2018).
- [33] H. Xiong, L.-G. Si, X.-Y. L, X. Yang, and Y. Wu, Opt. Lett. **38**, 353 (2013).
- [34] Z. X. Liu, H. Xiong, and Y. Wu, Phys. Rev. A **97**, 013801 (2018).
- [35] R. Holzwarth, T. Udem, T. W. Hänsch, J. C. Knight, W. J. Wadsworth, and P. S. J. Russell, Phys. Rev. Lett. **85**, 2264 (2000).
- [36] T. Udem, R. Holzwarth, and T. W. Hänsch, Nature **416**, 233 (2002).
- [37] T. R. Schibli, K. Minoshima, F. L. Hong, H. Inaba, A. Onae, H. Matsumoto, I. Hartl, and M. E. Fermann, Opt. Lett. **29**, 2467-2469 (2004).
- [38] T. J. Kippenberg, R. Holzwarth, and S. A. Diddams, Science **332**, 555 (2011).
- [39] P. Del’Haye, A. Schliesser, O. Arcizet, T. Wilken, R. Holzwarth, and T. J. Kippenberg, Nature **450**, 1214 (2007).
- [40] B. Zaks, R. B. Liu, and M. S. Sherwin, Nature **483**, 580 (2012).
- [41] S. O. Demokritov, V. E. Demidov, O. Dzyapko, G. A. Melkov, A. A. Serga, B. Hillebrands, and A. N. Slavin, Nature **443**, 430 (2006).